COBEM 2021 26th International Congress of Mechanical Engineering
November 22-26, 2021, Virtual Congress, Brazil

COB-2021-1023
CFD STUDY AROUND TANDEM WINGS FOR APPLICATION IN EVTOL AIRCRAFT

Leonardo Boff Breitenbach
Marco Antonio Sampaio Ferraz de Souza
URI - Universidade Regional Integrada do Alto Uruguai e das Missões - Câmpus de Erechim
Av. Sete de Setembro, 1621 - Fátima, Erechim - RS, CEP: 99709-910
breitenbach.bleonardo@gmail.com, marco@uricer.edu.br

João Luiz Rizzatti
URI - Universidade Regional Integrada do Alto Uruguai e das Missões - Câmpus de Erechim
Av. Sete de Setembro, 1621 - Fátima, Erechim - RS, CEP: 99709-910
joaolr20155@gmail.com

Abstract. *In recent years, different tandem wing configurations have been considered for a new class of aerial vehicles, EVTOL (Electric Vertical Takeoff and Landing) aircraft. The objective of this work is to study through CFD (Computational Fluid Dynamics) different tandem wing configurations in order to evaluate their aerodynamic efficiencies with large horizontal spacing and positive vertical spacing for an application focused on EVTOL aircraft concepts. In this context, the present work presents numerical simulations carried out using the commercial software Ansys Fluent 19.2 for six configurations, where the values of the horizontal distance between the wings were varied, as well as the dihedral of the rear wing and the aspect ratio of the front wing. Computational analyzes were performed by solving the Reynolds-averaged Navier–Stokes equations (RANS) and using the Spalart-Allmaras model, for a Reynolds number of 3.33x10^6, Mach number of 0.14 and flow angles ranging from -2 ° and 6 °. The results show that the front wing causes great interference with the flow around the rear wing, which worsens with increasing flow angle. The most influential parameter analyzed was the dihedral angle applied to the rear wing, which causes a gradual increase in the vertical distance between the fore wing and the rear wing from root to tip.*

Keywords: *Tandem wings, EVTOL, CFD, Aerodynamic efficiency*.

1. INTRODUCTION

In recent years, several companies from various sectors, including aeronautics, have sought to enable EVTOL (Electric Vertical Take-Off and Landing) aircraft for UAM (Urban Air Mobility). This search has been motivated by the need for faster transport, with greater efficiency and more accessible to the masses.

Uber, a company that operates in urban mobility, has been making great efforts to make possible the use of EVTOL aircraft. In October 2016, the company published a whitepaper, containing a comprehensive analysis around the characteristics that EVTOL aircraft must exhibit to become a viable urban transport mode. In this document, Uber highlights that EVTOL aircraft can bring several benefits when compared to helicopters (current urban air transport vehicles). According to the company, this new means of transport can provide faster transportation, with greater safety, greater energy efficiency, with lower noise levels, lower cost and no emission of polluting gases during operation.

The main challenges to be faced in EVTOL aircraft projects are to obtain a light and compact aircraft, while its operation must safely and efficiently unite the vertical takeoff and landing configurations together with the horizontal flight configuration, being the latter one of the biggest engineering problems, so it is difficult to get the best efficiency in the different flight modes.

Currently, the settings regarding the mode of operation of these aircraft can be summarized in three, namely:

a) Wingless: aircraft has an operating principle similar to the helicopter, where lift and displacement is exclusively generated by the action of rotors distributed over the fuselage;
b) Lift + Cruise: the aircraft uses rotor propulsion during vertical flight (takeoff and landing) and wings to generate lift during the cruise phase, while a second independent propulsion system is used for horizontal displacement;
c) Vectored Thrust: The aircraft uses the same propulsion system for takeoff, landing and cruise flight. For this, the engines are inclined to provide propulsion in the different modes of operation. In this configuration, the lift force during cruising is provided by the wings.

Each of the configurations presented has its own advantages and disadvantages, in the wingless configuration for example, it is easier to obtain a compact and efficient aircraft when hovering, however, as the rotors are always producing

an amount of thrust close to the mass of the aircraft, there is a lot of energy consumption in cruise flight. As generally most of the route taken by an aircraft takes place in cruise flight, this step has priority and, consequently, aircraft that use wings to generate lift during this phase, instead of rotors, usually have greater energy efficiency and greater autonomy.

Due to these characteristics, many of the developers have prioritized the design of EVTOL aircraft that use wings to generate lift and, among these, several have a tandem wing configuration. Some companies stand out with promising projects, some examples are: Airbus, Boeing, Embraer, Joby Aviation and Lilium.

Tandem wings are a very old concept in aviation, a landmark of this is the flight of the unmanned aircraft developed by Samuel Pierpont Langley that flew 1896. The tandem wing configuration is defined when an aircraft has two independent aerodynamic surfaces for the generation of lift , both with comparable proportions and normally positioned in two different planes, being thus separated by vertical and horizontal spacing (Minardo, 2014).

The tandem wing configuration consists of three design parameters in addition to those already existing for the case of a single wing, namely *St*, *G* and Δi_w. The diagram in Figure 1 shows a tandem wing configuration and its respective nomenclature.

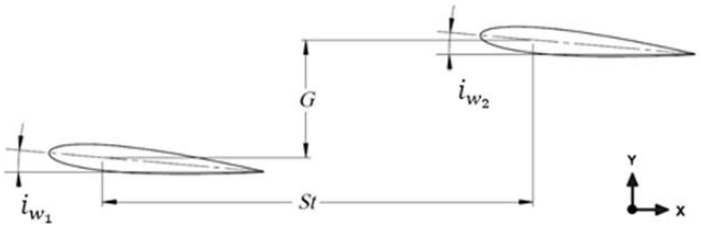

Figure 1. Nomenclature for tandem wing configuration.

The spacing represented by *St* corresponds to the horizontal distance between the two wings being measured the distance of ¼ of the wing's chord. The symbol *G* corresponds to the vertical distance between wing and wings by measuring ¼ of the chord of both wings. For the present work, *G* positive will be considered when the rear wing is above the front wing, however other authors may bring different definitions. Both *St* and *G* correspond to dimensionless distances being, *St* (*x/c*) and *G* (*y/c*). The symbol Δi_w represents the difference between the angles of incidence of the two wings, is also known as decalage angle, being defined by $\Delta i_w = i_{w_1} - i_{w_2}$, where i_{w1} and i_{w2} represent the angle of incidence of the front and rear wing respectively.

Despite being an unusual concept in aviation for some projects, it is possible that tandem wing configurations bring some advantages when compared to the conventional configuration (wing and tail). According to Raymer (2018) a supposed advantage concerns a 50% reduction in induced drag, however, as the same author emphasizes, for this to actually work it is necessary that each of the two wings have a length of a wingspan equal to that of a single wing, but with twice the aspect ratio.

Regarding flight safety, both tandem wings and canards (configuration where the front wing is smaller than the rear) can bring benefits. For this, the front surface must be designed in such a way that it stalls first than the rear surface, thus, in a critical flight condition even if the pilot is fully pulling the stick, the aircraft nose is lowered (Raymer, 2018) .

In addition to the aforementioned advantages, there are also some disadvantages associated with this type of configuration. In a tandem wing configuration the rear wing suffers from aerodynamic interference caused by the downdraft generated by the fore wing, so the flow experienced by the rear wing is directed at a small angle downwards. According to Raymer (2018), such an effect requires that the angle of incidence of the rear wing be increased, and this set of factors causes the support of the rear wing to be somewhat directed backwards and, as the lift is always perpendicular to the flow direction, the rear wing has a new drag component.

According to Raymer (2018), to minimize the effects of interference between the two wings, it is important to separate these surfaces as far as possible, both horizontally and vertically, with a configuration with a low front wing and a high rear wing being more advisable.

In addition to the points already highlighted, other aerodynamic, structural and stability characteristics restricted the use of tandem wings throughout the evolution of aviation, causing them to lose space for wing and tail configuration. Even so, in recent years, several authors have studied this topic, seeking to highlight the positive and negative characteristics of this type of configuration for different flow conditions. Some of these studies are cited in the sequence of this work.

Fanjoy and Dorney (1997) studied through numerical analysis the flow interactions around two NACA 0012 airfoils configured for *St* between 2 and 4, $G = 0$ and $\Delta i_w = 0$. The analyzes were performed for Mach numbers between 0.2 and 0.835 and Reynolds number of 6×10^6. The results showed that for the transonic regime the front wing helps to reduce the shock wave on the rear wing. The results also showed that for positive angles of attack, the aerodynamic efficiency (*L/D*) of the front wing increases while all aerodynamic forces on the rear wing decrease due to the occurrence of a reduction in the local angle of attack.

Using the Advanced Aircraft Analysis software, Pátek and Červinka (2007) performed a comparative study between a conventional aircraft configuration (wing and tail) and an aircraft configuration with tandem wings. For the tandem configuration, two wings were positioned in sequence so that the front wing is below the rear wing. The aircraft fuselage and the total area of the aerodynamic surfaces were kept equal for the two cases analyzed. The results showed that with the tandem wing configuration it is possible to achieve a higher maximum lift coefficient in certain flight conditions and also a lower overall drag in cruise flight. On the other hand, the results also indicate that stability for the tandem wing configuration is more critical.

Goetzendorf-Grabowski and Figat (2016) studied an EVTOL aircraft concept with tandem wings developed at the Warsaw University of Technology. The authors carried out investigations regarding the aerodynamic design and around the stability characteristics. To analyze the aerodynamics of the project, the MGAERO software was used and to assess the stability, the SDSA (Simulation and Dynamic Stability Analysis) software was used. The project proved to be promising, with the aircraft's performance characteristics being satisfactory. The stability characteristics showed some difficulty for the flight quality.

Alizadeh *et al*. (2019) designed an EVTOL aircraft with two wings of the same tandem shape, so that the rear wing is positioned at a point above the front surface. Through CFD analysis, the authors identified that due to the downward current effect caused by the front wing, there is a reduction in the pressure differential between the upper and lower surface of the rear wing, which reduces the lift coefficient of this surface when compared to the wing without interference.

Arnaud *et al*. (2019) developed the design of an EVTOL aircraft with tandem wings, where the front wing is below and has smaller proportions compared to the rear wing, this configuration of the front surface is named canard. The authors performed numerical simulations using the commercial Tranair software to analyze the influence of the canard on the flow over the rear wing. The results showed that the canard disturbs the flow around the rear wing, so that the effective angle of attack of the wing is decreased by 2° at the root, causing a decrease in lift for this region. Due to the influence of the canard the lift coefficient of the rear wing was reduced by almost 18%. The results also showed that the downward current effects start at the wing root and go up to a distance equal to half the span of the canard.

Addarkaoui *et al*. (2019) carried out the design of an EVTOL aircraft with tandem wings with the front wing of smaller proportion and positioned below the rear wing. The authors studied the flow around conceptually designed surfaces through numerical analysis using the Tranair software for a Reynolds number equal to 5.4×10^6. The results of the analyzes showed a reduction of 1/7 of the total lift of the wing with the use of the canard in relation to the wing without aerodynamic interference.

Cai *et al*. (2019) numerically investigated the influence of horizontal spacing *St* and vertical spacing *G*, from configurations of two symmetrical airfoils NACA 0012 in tandem, where *G* were varied from -4 to 4 and *St* from 1 to 4. The simulations were performed for two-dimensional flow using ANSYS Fluent 15 software with the Spalart-Allmaras turbulence model. The studied flow conditions were for Reynolds of 13.9×10^6 and Mach 0.6. Studies have shown that the lift coefficient of the rear wing is the most sensitive to variations in *St* and *G* spacing, while the front wing is little affected. The authors indicate that the value of *G* has greater aerodynamic influence compared to the *St* spacing.

Wang, Gan and Li (2020) carried out a study on the aerodynamic performance of a double-wing configuration with propeller-assisted lift increase. The wing configuration proposed by the authors is composed of a main wing and another auxiliary wing with the same span, but with a higher aspect ratio and positioned behind and above the main surface. For this configuration, the use of a single and two propellers positioned right in front of the auxiliary wing was investigated. The authors carried out the investigations through two different methods, where firstly, for faster analysis, they used a hybrid method PM/VPM (Panel Method/Vortex Particle Method) and later they used the MRF method (Multiple Reference Frame) through simulations in ANSYS software Fluent using the two-equation turbulence model kω-SST. The results showed that the proposed configuration increases lift and reduces drag, so that using a single propeller it was possible to obtain a 7.27% increase in efficiency compared to an isolated wing. Using two propellers there is still a 2.55% gain in efficiency compared to the case of a single propeller.

For EVTOL aircraft, such as the projects developed by Alizadeh *et al*. (2019), Arnaud *et al*. (2019) and Addarkaoui *et al*. (2019), the use of tandem wings can help make the aircraft more compact, safer and with more options for distribution of electric motors.

In this context, in the present study, numerical analyzes were performed in three dimensions for tandem wing configurations with a vertical spacing $G = 1$, two horizontal spacing values $St = \{3 \text{ and } 5\}$ and $\Delta i_w = 0$. Numerical analyzes were also performed for investigate the influence of the variation of wing design parameters, such as the use of a positive dihedral angle for the rear wing, which aimed to create an effect similar to the increase in vertical *G* spacing. Another parameter investigated was the increase in the aspect ratio of the front wing from the reduction of the chord length of the wing in question.

2. MATERIAL AND METHODS

The geometric model used for the numerical analysis was a rectangular semi-wing without geometric twist, without sweep and with all its extension being composed by the symmetric airfoil NACA 0012. The tip of the geometry has a

rounding generated by revolution. The semi-wing geometry was modeled using SOLIDWORKS software and is represented in Figure 2.

This model was chosen for having appropriate dimensions for the scope of this work and also for having experimental data available in the literature for the same analyzed flow conditions. These data are presented by Applin (1995), who studied the model from wind tunnel tests for a Reynolds range from $2.36x10^6$ to $4.71x10^6$ and Mach from 0.1 to 0.2 obtaining data for coefficients of pressure along the span of the geometry. Although Applin (1995) analyzed the model only for the case of a single wing, in the present work attention was focused on tandem wings, thus, the experimental data presented by the author were used basically in the steps of mesh refinement and validation of the numerical method.

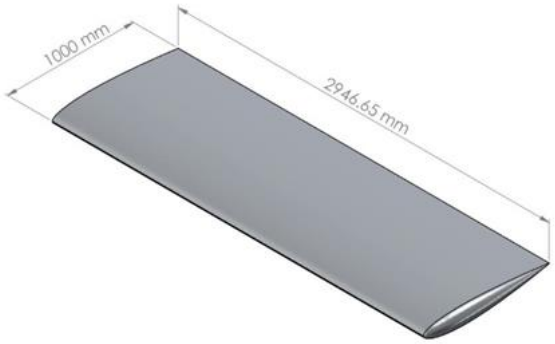

Figure 2. Semi-wing modeling.

After a study around the single wing, a second identical surface was then added characterizing the study of tandem wings, where the aim was to numerically analyze configurations in which the rear wing is positioned in a region above the front surface (positive *G*) and relatively high horizontal spacing *St* values. For the present study, the tandem wings were analyzed for: $G = 1$, $St = \{3 \text{ and } 5\}$ and flow angles equal to {-2°, 0°, 2°, 4° and 6°}, being classified as case 1 the configuration with $St = 3$ and case 2 the configuration with $St = 5$. Other 4 configurations were also analyzed, where two of them were for the spacing $St = 3$ and $St = 5$, adding a dihedral angle $\Gamma = 5°$ for the rear wing and the other two remaining configurations were for the spacing $St = 3$ and $St = 5$ with a 20% reduction of the front wing chord while maintaining its span (↓ Area and ↑ Aspect Ratio). These last four cases were only studied for the 0° flow angle. The tandem wing models analyzed using cases 1, 2, 3, 4, 5 and 6 are shown in Figure 3, Figure 4 and Figure 5, where *c* is the chord and *b* is the span of the wing (both measured in m). To make the visualization more intuitive throughout the work, the front wing in blue color and the rear wing in red color were considered.

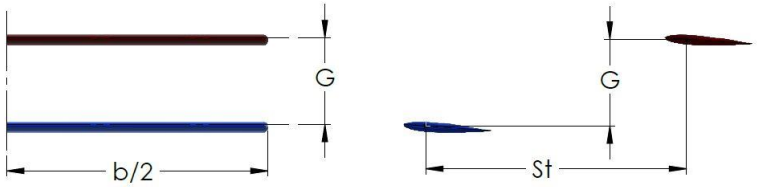

Figure 3. Configuration used in cases 1 and 2.

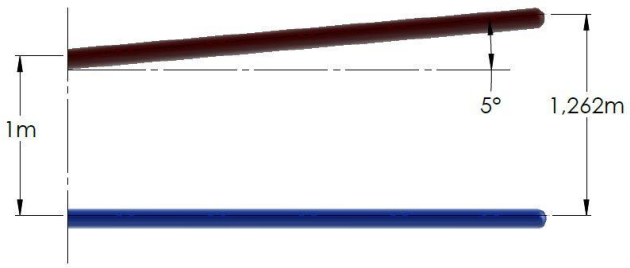

Figure 4. Configuration used in cases 3 and 4.

Through Figure 4, it can be seen that for the geometry in question, the application of a dihedral angle $\Gamma = 5°$ on the rear wing causes an increase in the vertical spacing of 26% for the wing tip in relation to the root.

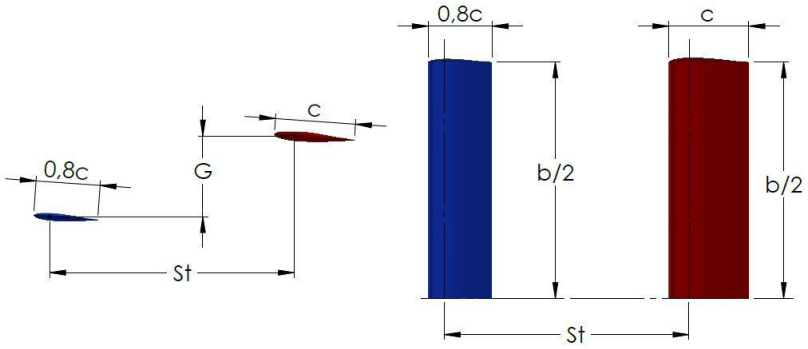

Figure 5. Configuration used in cases 5 and 6.

As the analyzes of the tandem configurations were carried out around wings composed of the symmetrical airfoil NACA 0012, which is not usual in transport aviation in general, these surfaces were then positioned for the same angle of incidence $i_{w1} = i_{w2} = 4°$, which generates an aerodynamic effect similar to a wing composed of a typical asymmetric airfoil used in general aviation at a zero incidence angle ($i_w = 0$). As the two wings were positioned for the same angle of incidence, the decalage angle is null, that is, $\Delta i_w = 0°$.

For the scope of this work, the problem was modeled by keeping the two wings fixed at the angle of incidence defined as if they were attached to a fuselage, thus, all numerical analyzes were performed by varying only the flow angle and not the angle of incidence of the wings. Thus, with the angle of incidence fixed at $i_w = 4°$ on the two surfaces, for the case of a flow angle equal to 6°, the angle of attack becomes a sum of the two values, being then 10°. Modeling the problem in this way, the numerical analyzes are performed as if the pitch angle of the aircraft was being varied, that is, for the flow angle of -2° the aircraft is simulated with a slight nose down and for the flow angle 6° simulates the aircraft with the nose up. This flow angle used in the numerical implementation of tandem wings was designated in this study for the symbol θ, and cases 1 and 2 were analyzed for $\theta = \{-2°, 0°, 2°, 4°, 6°\}$ and the other cases (3, 4, 5 and 6) were analyzed only for $\theta = 0°$.

The computational domain model along with the boundary conditions used are shown in Figure 6. For all cases studied the limits above, below, upstream and downstream of the semi-wing were modeled at a distance of eight chord lengths ($8c$), in order not to significantly influencing the flow around the wing or the wings and tandem. In all cases, for the surface of the wings, the boundary condition of no-slip wall was considered, and for the plane of intersection with the root of the wings, the symmetry condition was defined.

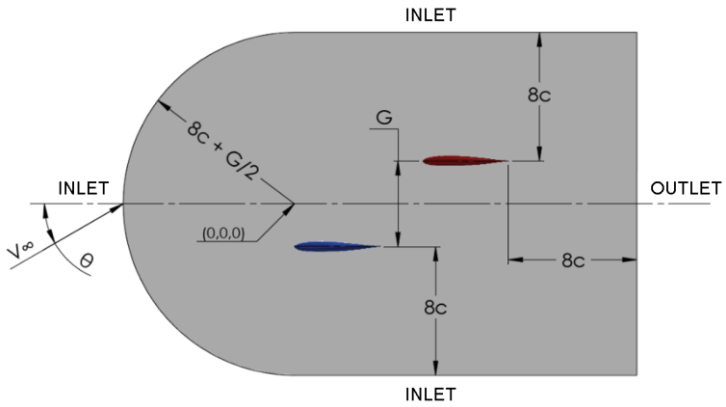

Figure 6. Computational domain and boundary conditions.

For all analyzed cases, the flow conditions presented in Table 1 were used.

Table 1. Flow conditions.

T [K]	ρ_∞ [kg/m³]	μ_∞ [N.s/m²]	M_∞	V_∞ [m/s]	Reynolds
288.16	1.23	1.79×10^{-5}	0.14	48.33	3.33×10^{6}

In Table 1, T is the fluid temperature (measured in K), ρ_∞ is the fluid density of the free stream (measured in kg/m³), μ_∞ is the dynamic viscosity of the fluid in the free stream (measured in N.s/m²), M_∞ is the Mach number of the free stream and V_∞ is the velocity of free stream (measured in m/s).

In all numerical analyses, the Reynolds-averaged Navier–Stokes equations (RANS) were used, with the solution being performed by the finite volume method. For turbulence modeling, the Spalart-Allmaras model was used. This model is widely used for analyzing external flows around airfoils, wings and other aerodynamic surfaces. The Spalart-Allmaras model is a model that solves a transport equation modeled for turbulent kinematic viscosity. According to Souza (2009), the Spalart-Allmaras model aims to improve the predictions obtained with algebraic models and provide a simpler alternative to the two-equation turbulence models. According to ANSYS (2013), this model was specifically designed for aeronautical and aerospace applications involving flow limited by walls, showing good results for boundary layers subject to adverse pressure gradients. According to Bardina, Huang and Coakley (1997), such a model does not require such a fine mesh in wall-limited flows as the two-equation turbulence models and demonstrates good convergence in simpler flows.

Numerical simulations were performed using ANSYS Fluent 19.2 software, using the pressure-based algorithm through a coupled formulation and with all second order spatial discretization schemes. Initialization was performed using the FMG (full multigrid) method. The numerical convergence criterion was defined for a maximum variation of $1x10^{-4}$ for all properties. This convergence criterion, although large, proved to be sufficiently precise during the validation step of the numerical method, thus, it was considered satisfactory for the scope of the present work.

The meshes were generated using the ICEM software where for all cases tetrahedral volumes were used, giving special attention to regions close to the surface of the wing, which received prism layers to better capture the flow effects under the boundary layer. The distance to the first prism layer was defined using y^+ calculations. It was decided to use 20 prism layers, with the first layer having a thickness of $2.2x10^{-5}$ m, which corresponds to $y^+ \approx 3$. After the first prism layer, the subsequent layers grow at a rate of 1.2. The meshes used for the validation of the numerical method and for the analysis of the tandem wings followed the same parameters.

For the validation of the numerical method, it was chosen to simulate the most critical flow condition to be analyzed, where the flow angle is more accentuated $\theta = 6°$, resulting in a total attack angle α of 10°. These conditions are shown in Table 2.

Table 2. Flow conditions for validation of the numerical method.

V_∞ [m/s]	M_∞	Reynolds	α [°]
48.33	0.14	$3{,}33x10^6$	10

Through the simulations, the distribution of the pressure coefficient in 10 different positions along the extension of the semi-wing was obtained. These data were compared with experimental data presented by Applin (1995) for the same flow conditions analyzed in the present work. The numerical results obtained in comparison with the experimental data of Applin (1995) are shown in Figure 7, where it can be seen that the numerical data are in good agreement with the experimental data for the entire extension of the geometry.

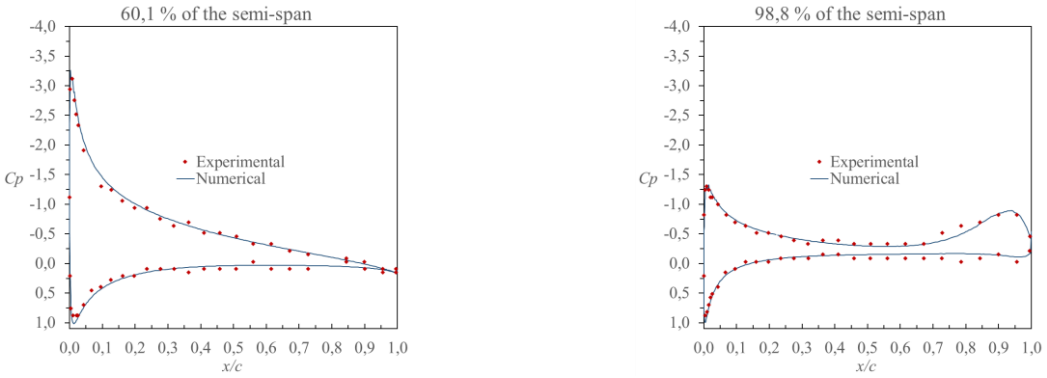

Figure 7. Plot of the pressure coefficient C_p on the single wing surface for $\alpha = 10°$.

3. RESULTS AND DISCUSSION

From Table 3, the total values for the lift and drag coefficients (C_L and C_D) and the efficiency (C_L/C_D) of each case are presented. All values are given for flow angles θ between -2° and 6°. Note that although the wings are composed of a symmetrical airfoil, for a flow angle of 0° the C_L values are far from being null, this is due to the fact that both wings

were fixed for an incidence angle of 4° in order to imitate a wing composed of an asymmetric airfoil at an incidence angle of 0°.

Table 3. C_L and C_D coefficients and C_L/C_D efficiency for St = 3 and St = 5.

	***St* = 3**			***St* = 5**		
***θ* [°]**	**C_L**	**C_D**	**C_L/C_D**	**C_L**	**C_D**	**C_L/C_D**
-2	0.260434	0.028035	9.29	0.263688	0.028136	9.37
0	0.523090	0.037414	13.98	0.528369	0.037605	14.05
2	0.780845	0.053249	14.66	0.782749	0.053599	14.60
4	1.031995	0.075543	13.66	1.027250	0.076119	13.50
6	1.274027	0.104216	12.22	1.255786	0.104851	11.98

Table 4 shows the percentages of reduction in lift coefficient and increase in drag coefficient of the rear wing in relation to the front wing for variations in the flow angle. It is noticed that for negative or very small runoff angles the greatest impact is the reduction in lift, however as the runoff angle increases, the impact due to the increase in drag is almost as large as that of the reduction in lift.

Table 4. Percentage of $\downarrow C_L$ and $\uparrow C_D$ of the rear wing in relation to the front wing for St = 3 and St = 5.

	***St* = 3**		***St* = 5**	
***θ* [°]**	**% ↓ C_L**	**% ↑ C_D**	**% ↓ C_L**	**% ↑ C_D**
-2	24.37	5.37	21.66	3.63
0	26.28	12.58	23.49	9.66
2	27.35	19.24	25.39	15.34
4	28.16	24.03	27.30	19.46
6	28.81	27.17	29.65	21.67

Table 5 shows the percentage contribution of each wing to total lift. Although the two wings have the same geometric shape and the same dimensions, through Table 5 we see that the forces generated by them are not the same, in which the largest tested flow angle (θ = 6°) showed the greatest imbalance.

Table 5. Wing contribution percentage in total C_L for St = 3 and St = 5.

	***St* = 3**		***St* = 5**	
***θ* [°]**	**% C_L Wing 1**	**% C_L Wing 2**	**% C_L Wing 1**	**% C_L Wing 2**
-2	56.94	43.06	56.07	43.93
0	57.57	42.43	56.65	43.35
2	57.92	42.08	57.27	42.73
4	58.19	41.81	57.90	42.10
6	58.41	41.59	58.70	41.30

Figure 8 shows the distribution of the pressure coefficient C_p along the surfaces for St = 3 and θ = 6°. Through the curves shown in Figure 8, it is observed that there was a great reduction in the C_p differential between the lower and upper surface of the rear wing compared to the front wing. For the wing tip region, specifically at 98.8%, it is noted that close to the trailing edge, the front wing has lower pressure coefficients, which indicates the formation of wing tip vortices with greater intensity compared to rear wing.

This set of aerodynamic effects observed in Figure 8, indicate that the rear wing experiences a very reduced flow angle compared to the flow angle experienced by the front wing, this effect is similar to that described by Alizadeh *et al*. (2019) and Arnaud *et al*. (2019). The reduction of this local angle of attack for the rear wing together with its impact on the C_p distribution can be seen in Figure 9, which shows the stream lines and C_p contours for St = 3 and θ = 6°. In Figure 9 it can be noted that for regions at 60.1% of the semi-span, the flow angle relative to the rear wing is much smaller than the flow angle relative to the front wing, which impacts a large difference between the C_p values of the front wing compared to the rear wing for these locations. The reduction in the C_p differential between the upper and lower surface observed for the rear wing in relation to the front wing, occurs due to a lower speed that develops mainly on the upper surface of the rear wing in relation to the speed that advances over the upper surface of the front wing. This lower speed is directly linked to the reduction in the angle of flow relative to the rear wing. This effect is proven by observing Figure 10, where the stream lines and velocity contours for the 60.1% position of the semi-span for the two wings are shown.

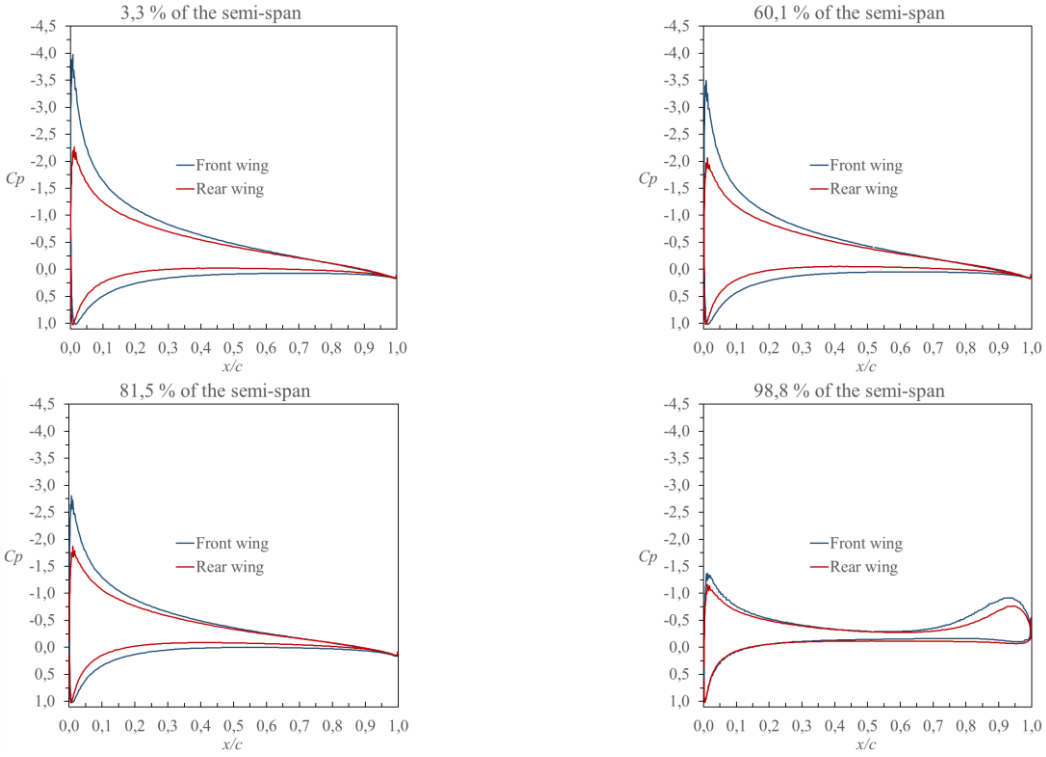

Figure 8. Plot of the pressure coefficient C_p for St = 3 and θ = 6° at different sections.

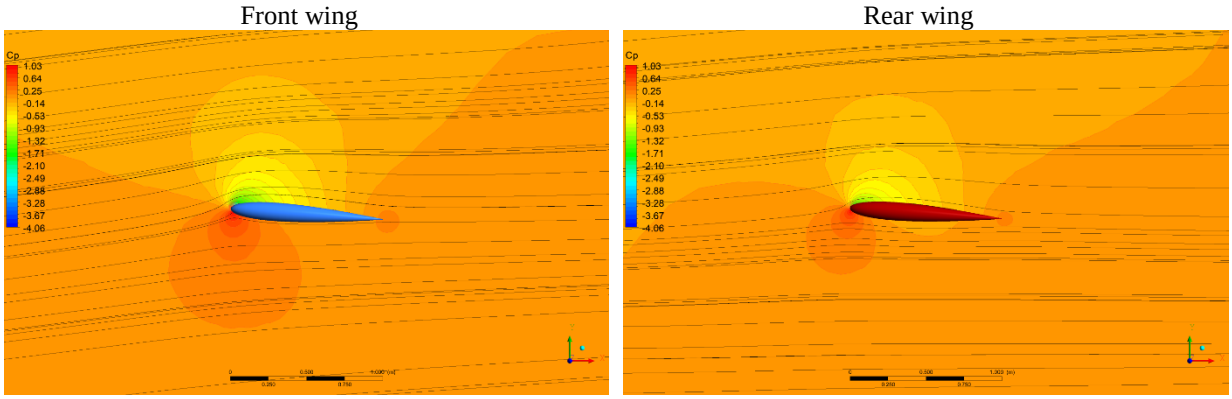

Figure 9. Stream lines and C_p contours for St = 3 and θ = 6° at 60.1% of the semi-wings.

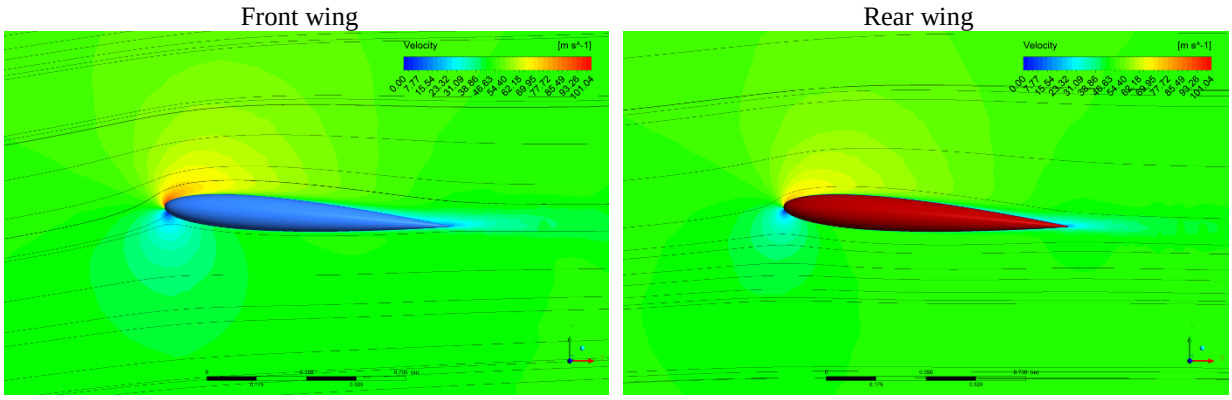

Figure 10. Stream lines and velocity contours for St = 3 and θ = 6° at 60.1% of the semi-wings.

In Figure 10, it can be seen that the flow angle relative to the rear wing is much smaller than the flow angle relative to the front wing. It is also noticed that because the rear wing experiences this reduced relative angle, the speeds around it are lower compared to the front wing. This phenomenon is the same as described by Fanjoy and Dorney (1997), where the authors indicate that for high Mach numbers, this lower speed can be seen as a benefit for minimizing the shock waves on the surface of the rear wing.

Figure 11 shows the aerodynamic efficiency curves for St = 3 and St = 5 as a function of the flow angle θ. Analyzing Figure 11, it is noted that for the flow angles of -2° and 0°, the configuration with St = 5 has a small aerodynamic efficiency advantage, while for the other flow angles (2°; 4° and 6°) the configuration with St = 3 presents better efficiencies and with a larger margin.

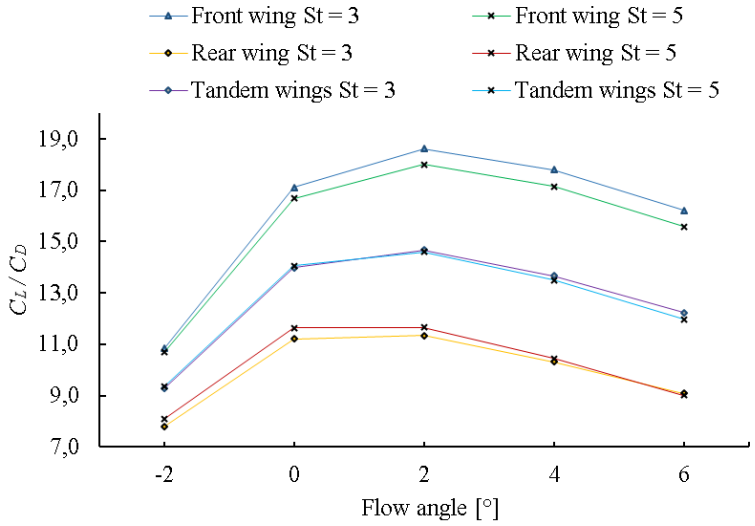

Figure 11. Aerodynamic efficiency of the wings for St = 3 and St = 5.

Through Figure 11, it can also be seen that for most of the analyzed flow angles, the rear wing presents a greater aerodynamic efficiency with the configuration of greater horizontal spacing (St = 5), except only for θ = 6°. In contrast, the front wing presents greater efficiency using the configuration with the smallest horizontal spacing (St = 3) for all analyzed angles. By means of these data it is clear that the horizontal spacing St has an influence on both the rear and front surfaces, where the higher value of St tends to favor the efficiency of the rear wing by providing a flow with less interference for this surface, on the other hand side the lower value of St favors the front surface.

The Table 6 shows the values for lift force L (measured in N), drag force D (measured in N) and aerodynamic efficiency L/D, for cases 1, 2 3, 4, 5 and 6 for θ = 0°. Through Table 6 it can be verified that the L values of the rear wing are always smaller when compared to the front wing and that the D values of the rear wing are always higher in relation to the front wing.

Table 6. Comparison between cases 1, 2, 3, 4, 5 and 6 for θ = 0°.

Nº case	$L_{wing\ 1}$ [N]	$L_{wing\ 2}$ [N]	L_{total} [N]	$D_{wing\ 1}$ [N]	$D_{wing\ 2}$ [N]	D_{total} [N]	L/D_{total}
1	1297.68	956.60	2254.27	75.85	85.39	161.23	13.98
2	1289.99	987.03	2277.02	77.30	84.76	162.06	14.05
3	1297.27	996.34	2293.61	75.89	85.46	161.36	14.21
4	1290.54	1026.10	2316.64	77.29	85.02	162.31	14.27
5	1097.68	1004.94	2102.63	64.40	84.38	148.78	14.13
6	1094.77	1029.62	2124.39	65.28	84.64	149.93	14.17

Analyzing the values presented in Table 6 and taking into account only the St spacing, it can be seen that the highest value (St = 5) represented by the cases with even numbers, presents the highest aerodynamic efficiencies compared to the lowest spacing value (St = 3), with case 2 being more efficient than case 1, case 4 more efficient than case 3 and case 6 more efficient than case 5. When taking into account the other parameters, such as the addition of the dihedral angle Γ=5° for the rear wing analyzed through cases 3 and 4 and the 20% reduction in the length of the front wing chord for the same span analyzed through cases 5 and 6, there is a better efficiency result for cases 3 and 4, with case 4 being the most efficient of all, with a lift to drag ratio of 14.27.

4. CONCLUSIONS

After this study, it can be concluded that the software used to generate the meshes and solve the problems, as well as the parameters of the meshes and the numerical method used, served well for the scope of this work, as demonstrated in the validation step, in that the data obtained are in agreement with the experimental data.

The results for cases 1 and 2 indicated a greater aerodynamic efficiency for $St = 5$ at flow angles between -2° and 0° while for the other analyzed angles (2°, 4° and 6°) the spacing $St = 3$ proved to be more efficient.

Analyzing the C_p distribution curves, the C_p contours and two-dimensional streamlines for the flow around the tandem wings in case 1($St = 3$) for the angle $\theta = 6°$, it was identified that the presence of the front wing has a great influence in the flow around the rear wing, drastically reducing the effective angle of attack to this surface.

For the analysis of cases 3 and 4, the best results were obtained in relation to aerodynamic efficiency, where the dihedral angle applied to the rear wing provided a gradual increase in the vertical spacing G from the root towards the wing tip. The dihedral increase for the rear wing proved to be the most influential parameter among the analyzed cases. For the flow angle $\theta = 0°$ among all cases, the highest efficiency was obtained for case 4 where $L/D = 14.27$. Cases 5 and 6 showed a small increase in efficiency compared to cases 1 and 2, however this small performance gain was followed by a large loss in lifting capacity. Nevertheless, the configuration of case 6 was the one that presented the best balance between the lift forces, with the rear wing generating around 48.5% of the total lift, which is beneficial from the point of view of stability and in addition, the higher aspect ratio combined with the higher effective angle of attack experienced by the front wing tends to cause that surface to stall first, which also contributes to the aircraft's stability and flight safety.

Although the analyzed geometries are not fully compatible with transport aviation due to the use of the NACA 0012 symmetric airfoil, even so the indications of increased or reduced efficiency due to variations in design parameters can be used as guidelines for future work applied to geometries more realistic.

5. REFERENCES

Addarkaoui, S. *et al*., 2019. “Graduate team aircraft design competition: Electric vertical takeoff and landing (E-VTOL) aircraft mistral air taxi”. AIAA Graduate Team Aircraft Design Competition 2018-2019.

Alizadeh, M. *et al*., 2019. “Spricho: An On-Demand Energy-Efficient E-VTOL Airtaxi”. AIAA Graduate Team Aircraft Design Competition 2018-2019.

ANSYS, Inc., 2013. *ANSYS Fluent Theory Guide*.

Applin, Z.T., 1995. “Pressure Distributions from Subsonic Tests of a NACA 0012 Semispan Wing Model”. Technical report, NASA TM 110148.

Arnaud, C. *et al*., 2019. “Duckampus: Autonomous electric vertical takeoff and landing aircraft”. AIAA Graduate Team Aircraft Design Competition 2018-2019.

Bardina, J. E., Huang, P. G., e Coakley, T. J., 1997. “Turbulence Modeling Validation, Testing, and Development”. Technical report, NASA TM 110446.

Cai, Y., Liu, G., Zhu, X., Tu, Q., Hong, G., 2019. “Aerodynamic Interference Significance Analysis of Two-Dimensional Front Wing and Rear Wing Airfoils with Stagger and Gap Variations”. Journal of Aerospace Engineering. Vol. 32, No. 6.

Fanjoy, D. W., Dorney, D. J., 1997. “A Study of Tandem-Airfoil Interaction in Different Flight Regimes”. American Institute of Aeronautics and Astronautics, AIAA Paper 1997-0515, pp, 1-18.

Goetzendorf-Grabowski, T., Figat, M., 2017. “Aerodynamic and Stability Analysis of Personal Vehicle in Tandem-Wing Configuration”. Proceedings of the Institution of Mechanical Engineers, Part G, Journal of Aerospace Engineering, Vol. 231, No. 11, pp. 214–2162.

Minardo, A., 2014. *The Tandem Wing: Theory, Experiments, and Practical Realizations* (in Italian). Master's Thesis, Aeronautical Engineering – Polytechnic from Milan, Milan, Italy.

Pátek, Z., Červinka, J., 2007. “Comparative Study of Conventional and Tandem - Wing Aircraft Configuration”. Czech Aerospace Proceedings, No. 1, pp. 6–8.

Raymer, D. P., 2018. *Aircraft design: A conceptual approach*. Sixth Edition. Virginia: AIAA.

Souza, M. A. S. F., 2009. *Numerical simulation of airfoil flow using turbulence model of an equation* (in Portuguese). Master's Thesis, Aerodynamics, Propulsion and Energy Area - Technological Institute of Aeronautics, São José dos Campos, Brazil.

Uber Elevate., 2016. *Fast-Forwarding to a future of on-demand Urban air transportation*.

Wang, H., Gan, W., Li, D., 2020. “An investigation of the aerodynamic performance for a propeller-aided lift-enhancing double wing configuration”. Aerospace Science and Technology, Vol. 105.

6. RESPONSIBILITY NOTICE

The authors are the only responsible for the printed material included in this paper.